Organic Carbon, Mercury, and Sediment Characteristics along a land – shore transect in Arctic Alaska

Frieda P. Giest[1,2], Maren Jenrich[1,3*], Guido Grosse[1,3], Benjamin M. Jones[4], Kai Mangelsdorf[5], Torben Windirsch[1,a], Jens Strauss[1*]

[1]Alfred Wegener Institute, Helmholtz Centre for Polar and Marine Research, Permafrost Research Section, Potsdam, Germany
[2]University of Potsdam, Institute of Environmental Science and Geography, Potsdam, Germany
[3]University of Potsdam, Institute of Geosciences, Potsdam, Germany
[4]Institute of Northern Engineering, University of Alaska Fairbanks, Fairbanks, Alaska, USA
[5]GFZ Helmholtz Centre for Geosciences, Organic Geochemistry Section, Potsdam, Germany
[a] now at Research Institute for Sustainability at GFZ, Potsdam, Germany

Correspondence to: Maren Jenrich (maren.jenrich@awi.de) and Jens Strauss (jens.strauss@awi.de)

Abstract. Climate warming in the Arctic results in thawing permafrost and associated processes like thermokarst, especially in ice-rich permafrost regions. Since permafrost soils are one of the largest organic carbon reservoirs of the world, their thawing leads to the release of greenhouse gases due to increasing microbial activity with rising soil temperature, further exacerbating climate warming. To enhance predictions of potential future impacts of permafrost thaw, a detailed assessment of soil characteristics' changes in response to thermokarst processes in permafrost landscapes are needed, which we investigated in this study in an Arctic coastal lowland. We analysed six sediment cores from the Arctic Coastal Plain of northern Alaska, each representing a different landscape feature along a gradient from upland to thermokarst lake and drained basin to thermokarst lagoons in various development stages. For the analysis, a multiproxy approach was used including sedimentological (grain size, bulk density, ice content), biogeochemical (total organic carbon (TOC), TOC density (TOCvol), total nitrogen (TN), stable carbon isotopes (δ^{13}C), TOC/TN ratio, mercury (Hg)), and lipid biomarker (*n*-alkanes, *n*-alkanols, and their ratios) parameters. We found that a semi-drained state of thermokarst lakes features the lowest OC content, and TOC and TN are generally higher in unfrozen deposits, hinting at a more intact state of organic matter. Indicated by the ACL, δ^{13}C and the P_{aq}, P_{wax} we found a stronger influence of aquatic organic matter (OM) in the OM composition in the soils covered by water, compared to those not covered by water. Moreover, it was indicated by the results of the δ^{13}C, TOC/TN ratio, and the CPI that the saline deposits contain stronger degraded OM than the deposits not influenced by saltwater. Additionally, we found positive correlations between the TOC and TOCvol and the Hg content in the deposits. The results indicate that thermokarst-influenced deposits tend to accumulate Hg during thawed periods and thus contain more Hg than the upland permafrost deposits that have not been impacted by lake formation. Our findings offer valuable insights into the dynamics of carbon storage and vulnerability to decomposition in coastal permafrost landscapes, reflecting the interplay of environmental factors, landform characteristics, and climate change impacts on Arctic permafrost environments.

1 Introduction

Climate warming represents one of the most pressing global environmental challenges of our time. Arctic regions are currently changing rapidly, since they experience some of the highest rates of impacts from climate change (Intergovernmental Panel on Climate Change (IPCC), 2022, 2023). Surface air temperatures in the Arctic increased up to four times the rate the global mean air temperature did over the last decades, a phenomenon referred to as Arctic amplification (Ballinger et al., 2023; Cohen et al., 2020; Rantanen et al., 2022). The local drivers of this amplification include the decrease of sea ice and snow cover, resulting in a decreased albedo, and a shift of cloudiness over the Arctic (Ballinger et al., 2023). Moreover, there are remote

drivers which contribute to the amplification, including an increased total water vapour in the Arctic atmosphere, due to an increased evapotranspiration and atmospheric moisture transport from the mid-latitudes and tropics, and accelerated heat from the atmosphere and the ocean (Cohen et al., 2020). As a result, surface temperatures in the Arctic during the winters in 2016 and 2018 were 6 °C above the average temperatures between 1981–2010 (IPCC, 2022).

One impact of this warming is the thaw of permafrost, which underlies large areas of the Arctic (Biskaborn et al., 2019; Smith et al., 2022). In some locations a total increase of 2–3 °C in the last 30 years was found within 10–20 m soil depth (Biskaborn et al. 2019). Permafrost has been identified as a large and vulnerable reservoir of organic carbon (OC) and due to climate change is considered a potential major future carbon source in the earth system (Hugelius et al., 2014; Mishra et al., 2021; Schuur et al., 2022). It is estimated that terrestrial deposits in permafrost regions store approximately 1460–1600 Gt carbon, which is about twice as much as is currently present in the atmosphere (Schuur and Mack, 2018; Strauss et al., 2025). As permafrost thaws, the soils can turn from a carbon sink to a carbon source (Schuur et al., 2009). Increased temperatures cause an acceleration of microbial activity and thus an increased decomposition of organic carbon in the deposits, leading to the release of greenhouse gases in the form of carbon dioxide and methane with the potential to further exacerbate climate change (Miner et al., 2022). In order to analyse the quality, hence the degree of decomposition, of organic matter (OM) in the different soils as well as differences in OM sources, lipid biomarkers can be used. Indices like the average chain length of n-alkanes (ACL), the carbon preferences index (CPI), and the higher plant index (HPA) can provide information about the source of the OM, as well as the level of degradation (Jongejans et al., 2020, 2021; Strauss et al., 2015).

Another consequence of permafrost thaw is the change of the landscape, for example due to melting ground ice causing surface subsidence and the development of thermokarst features (Grosse et al., 2013; Kokelj and Jorgenson, 2013). Around 20 % of the permafrost regions are affected by thermokarst processes, including the formation of thermokarst lakes and drained lake basins (Grosse et al., 2013; Jones et al., 2022; Olefeldt et al., 2016). In a coastal environment, increased coastal and riverbank erosion, sea level rise, higher water temperatures, and a reduced sea ice cover can lead to the inundation of thermokarst lakes and drained thermokarst lake basins by ocean water and the formation of thermokarst lagoons (Jenrich et al., 2021; Schirrmeister et al., 2018). These features add another complex setting of biogeochemical and hydrochemical processes in the transitional stage between terrestrial and marine environments, to the already diverse thermokarst landscapes (Schirrmeister et al., 2018).

In addition to the influence of permafrost thaw and the formation of thermokarst features on organic carbon characteristics in permafrost and thawed soils, changes in other biogeochemical characteristics may also occur, such as the relocation and release of mercury (Hg). It was found that considerable amounts of total Hg accumulated in the ice-rich permafrost region (Rutkowski et al., 2021). Since permafrost soils sequestered Hg bound in organic matter over centuries, it is estimated that the amount of Hg retained in permafrost regions is twice as high as in all other soils, the atmosphere, and the ocean combined (Schuster et al., 2018). Notably, the form of Hg released can significantly influence its environmental impact, as methylmercury is particularly toxic to humans and wildlife. Additionally, there is often a correlation between total organic carbon (TOC) and total mercury (e.g., Chakraborty et al., 2015), highlighting the interplay between organic matter and Hg dynamics in permafrost regions. Therefore, Hg remains a notable environmental concern in the Arctic region, as elevated exposure—particularly to methylmercury—can impact human health and have negative effects on ecosystems (Rydberg et al., 2010; Smith-Downey et al., 2010).

In this study, we use a multiproxy approach to characterise OM in different landscape features of a coastal permafrost lowland along a gradient from upland to thermokarst-affected terrains (lakes and drained basins) to thermokarst lagoons representing a transition from terrestrial to marine environments on the Arctic Coastal Plain of northern Alaska. We aim to answer how OC characteristics and correlating biogeochemical parameters change with permafrost degradation and coastal saltwater inundation.

2 Study area and study sites

The study area is located in the Arctic coastal plain of northern Alaska, north of the Teshekpuk Lake (figure 1). The North Slope, an area framed by the Brooks Range in the south and the Beaufort Sea in the north, encompasses a diverse geology including deposits originated in the North American craton, passive margin sediments, rift sediments, pelagic sediments, volcaniclastics and deposits from the foreland basin (Jorgenson et al., 2011). Surface deposits in the study area consist of glacio-marine silts, marine sands, alluvial sands and silts from the Holocene and mid-Quaternary epochs (Jorgenson and Grunblatt, 2013).
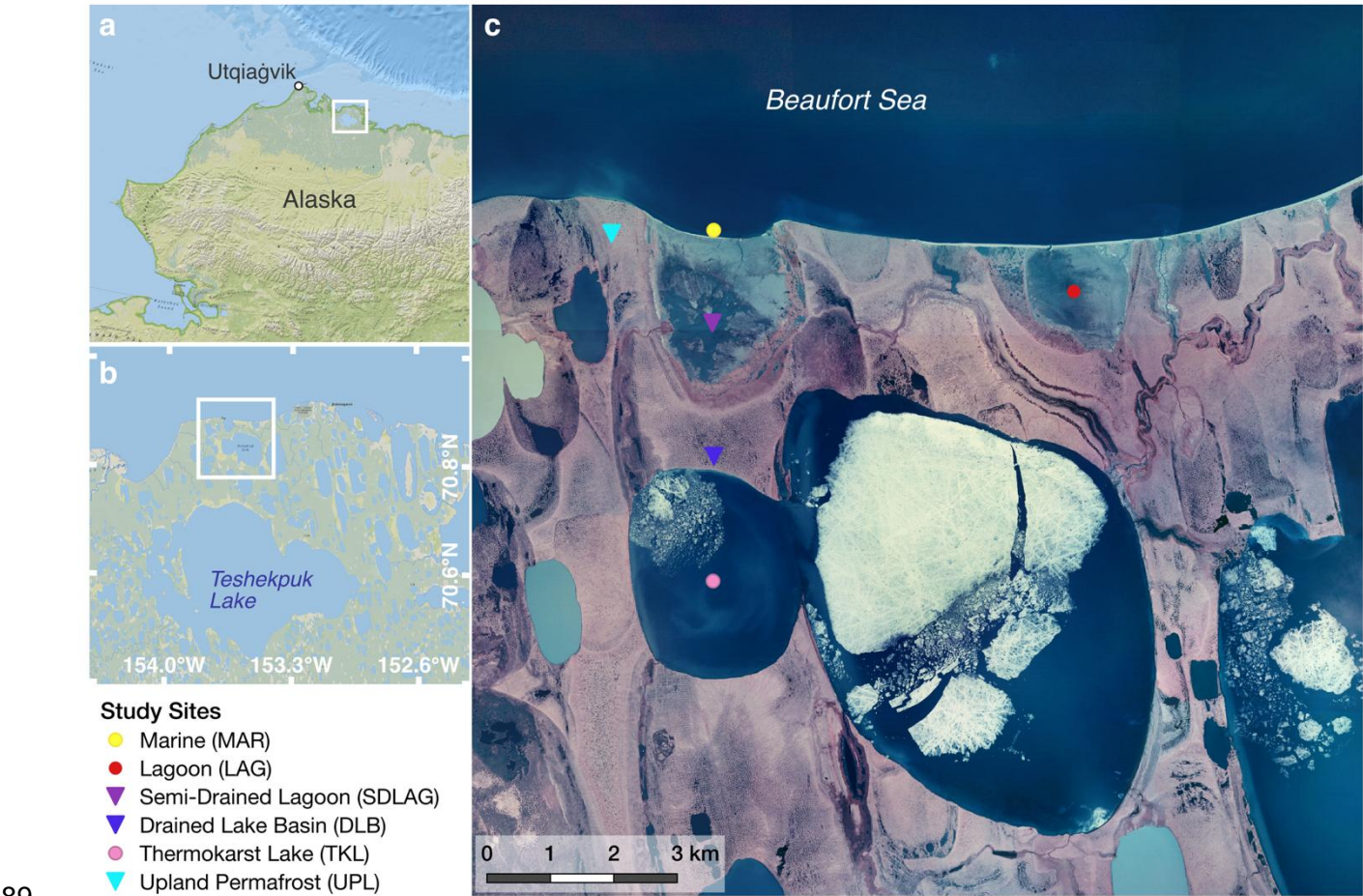
Figure 1: Map of the study sites located north of the Teshekpuk Lake in northern Alaska. (a, b) Close-up of the study area, with the coring locations marked as dots (unfrozen deposits) and triangles (frozen deposits) (c). Sources: a, b: ESRI, c: Color infrared ortho aerial image (U.S. Geological Survey, Earth Explorer, 2002); for relative positions of the individual study sites, please refer to figure S1 in the supplementary material.

The climate in the region is cold and arid, with a mean annual temperature of -12 °C and a mean annual precipitation of 115 mm per year (Jorgenson et al., 2011). The soil composition in the area is intrinsically tied to the presence of continuous permafrost, with an interplay of low temperatures, impeded drainage, freeze-thaw dynamics, cryoturbation, and ground ice aggregation, collectively shaping its characteristic. The presence of 200 to 400 m thick continuous permafrost also led to the formation and preservation of one of the largest wetland complexes in the Arctic, which despite the cold and arid climate also lead to the accumulation of high OC contents in the soils (Jorgenson et al., 2011; Wendler et al., 2014). Moreover, the landscape is continuously transformed by thawing permafrost and melting ground ice, leading to ground subsidence and the formation of numerous thermokarst lakes and drained lake basins (Arp et al., 2011; Fuchs et al., 2019; Jones and Arp, 2015; Jorgenson and Shur, 2007; Wolter et al., 2024). Coastal erosion along the Beaufort Sea coast in this area is among the highest observed in the Arctic, resulting in the drainage of lakes and formation of thermokarst lagoons and embayments, and is currently accelerating further (Jones et al., 2009, 2018; Jones and Arp, 2015).

3 Material and Methods

3.1 Fieldwork

The fieldwork was performed during a joint German-US expedition to the Teshekpuk Lake area in Alaska in April 2022. For this study six soil cores were selected following a transect from inland to coast, with all core sites being located in close distance to each other (Figure 1). All sample sites represent different landscape features of a coastal thermokarst affected permafrost landscape scape, with the chosen transect describing the transformation pathway from a terrestrial permafrost landscape into a coastal marine environment, following thaw and erosion processes (Jenrich et al., 2021). Three of the cores were frozen: from a permafrost upland (UPL; length 203 cm), a drained thermokarst lake basin (DLB; length 219 cm), and a semi-drained lagoon (SDLAG; length 183 cm). Three other cores were unfrozen: from a thermokarst lake (TKL; length 50 cm), a thermokarst lagoon (LAG; length 31 cm), and marine deposits (MAR; length 12 cm) (figure S1 in the supplements). For reference, all subsample depths are given in centimetres below surface level (cm b.s.l.). The unfrozen sediment cores were sampled using a Push Corer [Ø 6 cm], the frozen sediment cores were sampled using a SIPRE Corer [Ø 7.6 cm]. The frozen sediment cores were kept frozen at -20 °C, while thawed samples were packed and cooled at +4 °C for transport to AWI Potsdam, where all further analyses were conducted.

3.2 Laboratory analysis

The cores were subsampled in intervals of 5 to10 cm. For the biomarker analysis, three to four samples of the longer, frozen cores and one to two samples of the shorter, unfrozen cores were selected, evenly distributed over the length of the cores. In preparation for further analyses, water for hydrochemical analysis was extracted, and subsequently all samples were freeze-dried, determining their weight before and after this process to calculate water respectively ice content. A more detailed description of the methods used in the laboratory is given in the supplements (Sect. S1 in the supplements).

3.2.1 Sedimentological analysis

The sedimentological analysis was mainly the measurement of grain size distribution (GSD).

These measurements were carried out using a Malvern Mastersizer 3000 with a Malvern Hydro LV wet-sample dispersion unit, measuring in a range between 0.01–1000 µm. All grain size statistics were calculated using the software GRADISTAT (Blott and Pye, 2001) (Sect. S1.1 in the supplements).

3.2.2 Biogeochemical analysis

For biogeochemical analysis, all samples were homogenised using a planetary mill [FRITSCH pulverisette 5]. The determination of the total organic carbon content (TOC) was carried out using an ELEMENTAR soliTOC cube elemental analyser, measuring TOC and total inorganic carbon (TIC) via pyrolysis and gas analysis. Using a temperature ramping program to distinguish between TOC and TIC, the device was heated to 400 °C for 230 seconds (TOC), and subsequently heated to 600 °C for 120 seconds (TIC). Third heating stage was 900 °C for 150 seconds to ensure complete combustion of inorganic carbon compounds.

The carbon density (TOCvol) of each sample was determined using the bulk density and the TOC content. It was calculated using the following equation (1) (Strauss et al., 2015).

$$TOC_{vol}[kg\ m^{-3}] = BD[kg\ m^{-3}] \cdot \frac{TOC\ [wt\%]}{100} \tag{1}$$

The total nitrogen (TN) content was measured using an ELEMENTAR rapid MAX N exceed elemental analyser with a peak combustion temperature of 900 °C.

142 From the measured TOC and TN contents the TOC/TN ratio was calculated. This ratio provides information on the sources

143 and the degradation level of the organic matter (OM) in the sediment, with high values indicating a higher share of terrestrial

144 source material or well-preserved OM and low values indicating a higher share of aquatic sources or a high level of degradation

145 of OM (Andersson et al., 2012; Meyers, 1997).

146 The measurement of the total mercury (Hg) content of the sediment samples was carried out using the direct mercury analyzer

147 DMA-80 EVO.

148 The measurement of the $\delta^{13}C$ signature of bulk organic matter, as a paleoenvironmental indicator, can also provide information

149 on the sources of OM and its degree of decomposition. It is mainly determined by photosynthetic processes, but also by other

150 factors like atmospheric CO_2, temperature, and water stress (Andersson et al., 2012). As the first step of the analysis, carbonates

151 were removed from the samples using hydrochloric acid. Subsequently, the measurement was carried out using a ThermoFisher

152 Scientific Delta-V-Advantage gas mass spectrometer with a FLASH elemental analyser EA 2000 and a CONFLO IV gas

153 mixing system. The isotope ratio was determined in relation to the Vienna Pee Dee Belemnite standard [‰ vs VPDB], and the

154 instrumental measurement accuracy is ± 0.15 ‰.

155 **3.2.3 Lipid biomarker analysis**

156 **Extraction, measurement and analysis**

157 Subsamples for lipid biomarker analysis were freeze-dried and homogenised. Lipid biomarkers were then extracted from

158 approximately 8 g of sample material using accelerated solvent extraction (ASE; ThermoFisher Scientific Dionex ASE 350)

159 with dichloromethane/methanol (DCM/MeOH 99:1). During extraction, samples were held in a static phase for 20 min at

160 75.5 °C and 5 MPa. For the subsequent analysis, 5α-androstane as a reference for *n*-alkanes in the aliphatic fraction, and 5*a*-

161 androstan-17-one as a reference for *n*-alkanols in the neutral NSO (nitrogen, sulphur, and oxygen containing) fraction were

162 added. Resolved samples were then fractionated into an aliphatic, aromatic and NSO fraction using a medium pressure liquid

163 chromatography (MPLC) system (Radke et al., 1980). Subsequently, the NSO fraction was separated into an acidic and neutral

164 polar fraction by a manual KOH column separation. In preparation for the measurement the neutral NSO fraction was silylated

165 by adding 50 µl DCM and 50 µl N-Methyl-N-(trimethylsilyl)trifluoroacetamide (MSTFA) and heated at 75 °C for one hour.

166 The measurement of *n*-alkanes in the aliphatic fraction and *n*-alkanols in the neutral NSO fraction was performed using gas

167 chromatography-mass spectrometry (GC-MS; Thermo Scientific ISQ 7000 Single Quadrupole Mass Spectrometer with a

168 Thermo Scientific Trace 1310 Gas Chromatograph). The GC-MS system was operated with a transfer line temperature of

169 320 °C and an ion source temperature of 300 °C. Ionisation was achieved using an ionisation energy of 70 eV at 50 µA. The

170 full scan mass spectra (m/z 50 to 600 Da, 2.5 scans s^{-1}) was analysed using the software XCalibur. The *n*-alkanes and *n*-alkanols

171 were quantified by comparing their peak areas with those of the internal standards.

172 **Biomarker indices**

173 In total, five indices were calculated from the measured lipid biomarker concentrations. Three of these indices, calculated from

174 the *n*-alkane concentrations, provide information on respective sources of the OC.

175 The first index was the average chain length (ACL) of *n*-alkanes C$_{23-33}$, calculated following equation 2 where *i* is the carbon

176 number and *C* is the concentration (Poynter and Eglinton, 1990; Strauss et al., 2015).

177 $$ACL = \frac{\sum i \cdot c_i}{\sum c_i}$$ (2)

178 A change of the ACL can indicate a change of the OC sources and thus a change of input vegetation type to the soil profile

179 (Schäfer et al., 2016). The long chain odd-numbered *n*-alkanes are mainly produced by terrestrial plants like bryophytes (*n*-

180   C$_{23}$ & n-C$_{25}$), grasses (n-C$_{31}$ to n-C$_{33}$), or originate from terrestrial plant leaf waxes (n-C$_{27}$ to n-C$_{29}$) (Haugk et al., 2022; Zech

181   et al., 2010).

182   The second and third indices are the P_{aq} (ratio of aquatic to terrestrial plant material, equation 3) and the P_{wax} (ratio of terrestrial

183   plant waxes to total hydrocarbons, equation 4), two ratios that can be used as proxies for the intensity of aquatic influence on

184   the sediments and to differentiate between aquatic and terrestrial plant input (Thomas et al., 2023; Zheng et al., 2007).

185   $$P_{aq} = \frac{C_{23}+C_{25}}{C_{23}+C_{25}+C_{29}+C_{31}} \tag{3}$$

186   $$P_{wax} = \frac{C_{27}+C_{29}+C_{31}}{\sum odd\ C_{23-31}} \tag{4}$$

187   With the P_{aq}, developed by Ficken et al. (2000) it is possible to distinguish between submerged and floating macrophytes, with

188   values between 0.4 and 1, emergent macrophytes, with values between 0.1 and 0.4, and terrestrial plants, values < 0.1, as a

189   source for OC in the soil. Since this index and its thresholds were developed in tropical regions, the P_{wax} was additionally used

190   in this study, as seen in Jongejans et al. (2020). The P_{wax}, developed by Zheng et al. (2007), indicates the relative proportion

191   of waxy hydrocarbons from emergent macrophytes and terrestrial plants to total hydrocarbons (Zheng et al., 2007).

192   The following two indices are used to provide information on the level of degradation of the OC in the soils. The first index is

193   the Carbon preference index (CPI) of n-alkanes, introduced by Bray and Evans (1961). As a measure of alteration of OC,

194   values of the CPI decrease with the degradation of OC in the soil (Marzi et al., 1993; Strauss et al., 2015). The calculation in

195   this study was carried out using the equation introduced by Marzi et al. (1993), with a chain length interval of C$_{23-33}$ (equation

196   5).

197   $$CPI_{23-33} = \frac{\sum odd\ C_{23-31} + \sum odd\ C_{25-33}}{2 \cdot \sum even\ C_{24-32}} \tag{5}$$

198   The second index as a measure of level of degradation of OC, introduced by Poynter (1989) is the higher plant alcohol index

199   (HPA). As a basis of this index, it is assumed that the input ratio of n-alkanols and n-alkanes into a sedimentary environment

200   is constant. Therefore, the ratio should depend on the extent of degradation, and since the n-alkanols are preferentially degraded

201   over the n-alkanes or degraded to n-alkanes due to defunctionalisation, the ratio decreases with ongoing degradation (Poynter

202   and Eglinton, 1990). The index was calculated using the following equation (6) (Poynter and Eglinton, 1990).

203   $$HPA = \frac{\sum(n-alkanols\ C_{24}, C_{26}, C_{28})}{\sum(n-alkanols\ C_{24}, C_{26}, C_{28}) + \sum(n-alkanes\ C_{27}, C_{29}, C_{31})} \tag{6}$$

204   **3.3 Statistical analysis**

205   The statistical analysis of the data included the analysis of central tendencies of the measured parameters across the different

206   cores, and the comparison of unfrozen and frozen deposits, as well as saltwater influenced sites, and those not influenced by

207   saltwater. Central tendencies analysis across the different cores was only applied to the SDLAG, TKL, DLB, and UPL cores,

208   since the LAG and MAR cores had a too small sample size. After testing and disproving a normal distribution of the data, the

209   nonparametric Kruskal-Wallis rank sum test was chosen to compare the data of the four different sites. For an additional pair-

210   wise comparison of cores the Mann-Whitney-Wilcoxon test was used. In addition, it was tested if there are statistically

211   significant differences between deposits that are influenced by saltwater (MAR, LAG, SDLAG) and deposits that are not

212   influenced by saltwater (DLB, TKL, UPL) and the frozen (SDLAG, DLB, UPL) and unfrozen (MAR, LAG, TKL) cores, using

213   the Mann-Whitney-Wilcoxon test. All tests of the central tendency analysis were carried out using R (script in Sect S4.1 &

214   S4.2 in the supplements).

215   To test the data for existing correlations between the different measured parameters, a correlation matrix was created in R

216   (script in Sect. S4.3 in the supplements). The calculation of the correlation was carried out after Pearson. The finished plot of

217   the correlation matrix only shows correlations with a significance of $p < 0.05$.

4 Results

4.1 Sedimentology

The upland permafrost core (UPL) is generally dominated by silt (figure 2), as are the sediment samples of the thermokarst lake (TKL) but with a slightly higher share of silty material. Similar results are present for the drained lake basin core (DLB), with all said cores being homogeneous over the whole length (figures 2, 3). The GSD of the semi-drained lagoon (SDLAG) has a shift from higher shares of coarser grain sizes in the range of fine sand and more silty material found below 100 cm b.s.l., while the upper part reaches towards silty and clayish material. The deposits of the intact lagoon (LAG) are again dominated by silt (figure 2). The deposits, namely one sample, of the marine core (MAR) shows a bigger sand portion of 58.5 %, and represents generally the coarsest grain sizes among the six studied cores (figure 3). For more details, please see the supplementary figures S1 -S3, as well as the published measurement data (Giest et al., 2025).
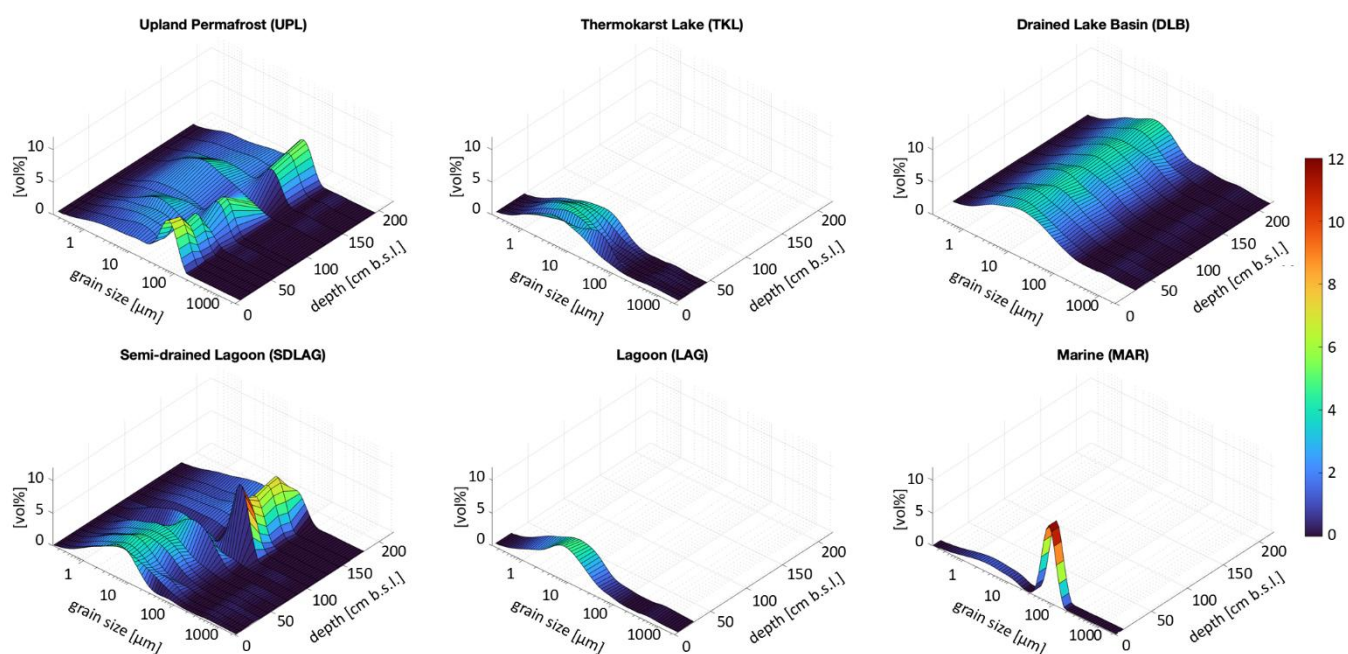
**Figure 2: Three-dimensional grain size distributions over depth [cm] of a land-sea transect**: a) upland Permafrost, b) thermokarst lake, c) drained lake basin, d) semi-drained lagoon, e) intact lagoon and f) marine profiles. The Colours represent the share [%] of the grain sizes [µm] with dark blue representing 0 % and red representing 10 %.

4.2 Biogeochemistry

The DLB core shows the strongest variations in the TOC content, ranging from 2.94 wt% to 37.62 wt%, with a mean of 7.57 wt% (median 3.26 wt%) (figure 3). The UPL core also shows strong variations in the TOC content, peaking at 20.42 wt% at a depth of 56 cm b.s.l., with a mean of 4.66 wt% (figure 3). In contrast, the TKL sediment core shows a smaller range in the TOC content, between 4.63 wt% and 6.23 wt% (mean 5.37 wt%) (figure 3). It is significantly higher than the TOC content in the upper part of the UPL deposits. The two samples from the LAG plot within the lower end of the range of the TKL deposits, with TOC contents of 4.63 wt% and 4.09 wt% (figure 3). Above 40 cm the TOC content of the SDLAG core varies between those of the UPL and TKL deposits, below it has a consistently lower TOC contents than the other deposits, with a mean of 2.37 wt%, which is significantly lower than in the DLB and TKL samples (figure 3). Additionally, the sample of the MAR deposits has a very low TOC content of 1.3 wt% (figure 3).

243 The highest TOCvol was determined in the TKL deposits, with a mean of 48.02 kg m^{-3} (figure S3). It is significantly higher

244 than in the SDLAG deposits (mean 32.23 kg m^{-3}) and the DLB deposits, with the lowest mean of 25.06 kg m^{-3}, both with

245 strong variations in the TOCvol over depth (figure 3 & S3). The strongest variation in the TOCvol is shown by the UPL core,

246 ranging between 6.79 kg m^{-3} and 119.7 kg m^{-3} (figure 3). The mean TOCvol of the UPL deposits of 36.66 kg m^{-3} is relatively

247 high (figure S3). The TOCvol of the marine sample is again relatively low with 20.86 kg m^{-3} (figure S3).
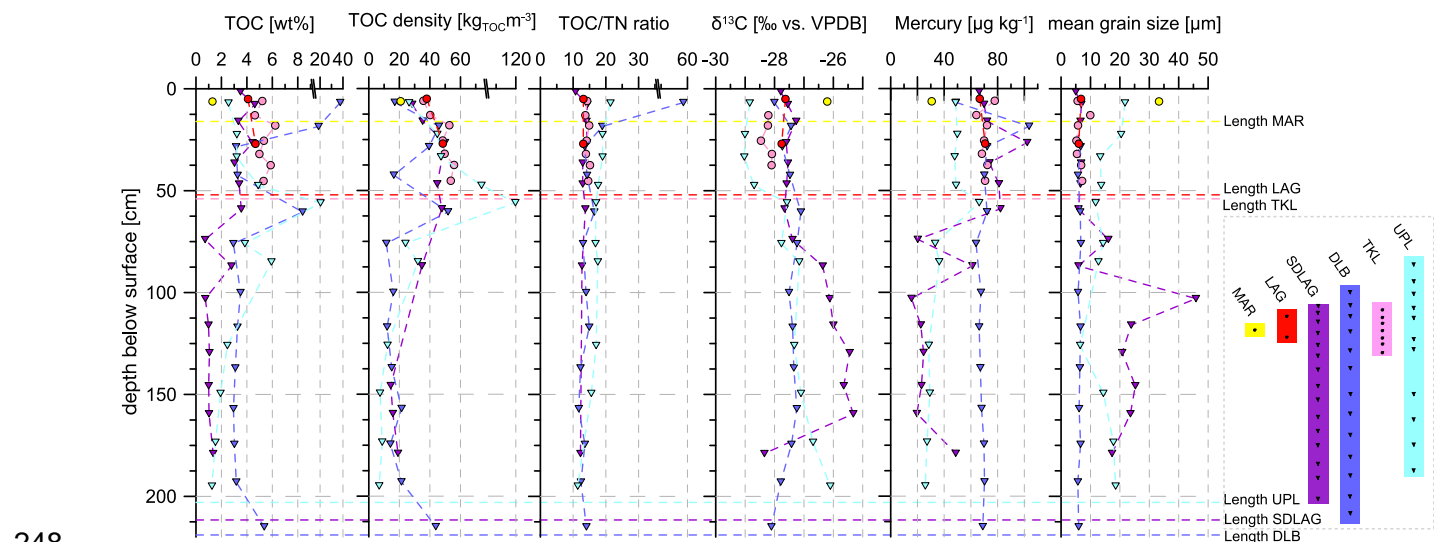
249 **Figure 3: Summary of the biogeochemical parameters:** total organic carbon (TOC) in weight percent[wt%], TOC density [kg$_{TOC}$cm^{-3}],
250 total organic carbon/total nitrogen ratio (TOC/TN ratio), stable carbon isotope ratio (δ^{13}C) per mil relative to Vienna PeeDee Belemnite
251 standard [‰ vs. VPDB], Mercury [µg kg^{-1}] and mean grain size [µm] of the UPL, TKL, DLB, SDLAG, LAG, and MAR profiles, with
252 circles for unfrozen sediments and triangles for frozen sediments. Core abbreviations: UPL: upland permafrost; TKL: thermokarst lake;
253 DLB: drained lake basin; SDLAG: semi-drained lagoon; LAG: lagoon; MAR: marine. Split x axis for TOC, TOC density and TOC/TN ratio.

254 The TOC/TN ratio is highest in the UPL deposits (mean 17.23), which is significantly higher than in all thermokarst influenced

255 deposits (figure 3). The lowest TOC/TN ratios were measured in both lagoonal sites, with a mean of 13.1 in the SDLAG core

256 (figure 3). The TOC/TN ratios of the SDLAG core are additionally significantly lower than TOC/TN ratios of the TKL

257 deposits, with a mean of 14.39 (figure 3). The DLB core shows the highest ratio of 58.46 in the uppermost sample and a strong

258 decrease in the deeper samples resulting in a mean of 17.5 (median 13.95) (figure 3 & S3). The TN content of the MAR sample

259 below the detection limit resulted in no TOC/TN ratio.

260 Strongest variations in the δ^{13}C ratio were measured in the UPL (−26.1 to −29 ‰) and SDLAG (−25.3 to −28.3 ‰) deposits

261 (figure 3). It is lowest, around −29 ‰, in the upper 50 cm of the UPL core and increases in the deeper part of the core (mean

262 −27.8 ‰) (figure 3). Both the DLB (mean −27.5 ‰) and the SDLAG (mean −26.9 ‰) deposits have significantly higher δ^{13}C

263 ratios than the TKL deposits, with the lowest mean δ^{13}C ratio of −28.2 ‰ (figure S3).

264 The mercury (Hg) analysis of the different cores shows that the thermokarst influenced deposits have higher Hg concentrations

265 compared to the UPL deposits. Significant differences in the Hg content were observed between the DLB and UPL deposits,

266 as well as between the TKL and UPL deposits, with the UPL samples having significantly lower Hg concentrations (figure

267 S3). The median Hg content of the TKL samples (70.63 µg kg^{-1}) is nearly twice as high as the median of the UPL samples

268 (36.34 µg kg^{-1}). Furthermore, the Hg levels of the two samples of the LAG core are in the same range as in the TKL samples

269 (figure 3). The SDLAG profile shows the largest variations in the Hg content across the samples and has no significant

270 differences to the other cores (figure 3 & S3). For more details, please see the published dataset (Giest et al., 2024b).

4.3 Biomarker

4.3.1 Organic carbon sourceindicating indices

The average chain lengths of *n*-alkanes (ACL) are highest in the three samples of the UPL core, with the highest value of 28.73 in the sample from the middle part (figure 4). Lowest values have been detected for the LAG and the MAR samples, with the lowest from the MAR core (26.2) at a depth of 6.25 cm b.s.l. (figure 4). All cores with more than one sample show higher ACL values in deeper part of the core (figure 4).

As shown in figure 4, the highest P_{aq} values were measured in the MAR sample and the uppermost DLB sample, both having a P_{aq} of 0.66. The MAR sample also has the lowest P_{wax} of 0.52 indicating together with the P_{aq} an aquatic influence on the OM composition (figure 4). Also, the uppermost DLB sample shows a relatively low P_{wax} of 0.56 (figure4). Other samples with high P_{aq} and low P_{wax} are both LAG samples, with a P_{aq} between 0.61 and 0.64 and a P_{wax} between 0.54 and 0.55, and the uppermost SDLAG sample with a P_{aq} of 0.62 and a P_{wax} of 0.53 (figure 4). The highest P_{wax} values were calculated for all UPL samples, ranging between 0.76 and 0.74 (figure 4). At the same time, they show the lowest P_{aq} values, varying between 0.31 and 0.39 (figure 4). Another sample with a high P_{wax} of 0.73 and a low P_{aq} of 0.41 is the DLB sample from a mean depth of 65.25 cm b.s.l. (figure 4). Overall, the data shows two end members, the marine sample with the most aquatic OM source and the upland permafrost samples with the most terrestrial OM source with the samples from the other location distributed between the two.
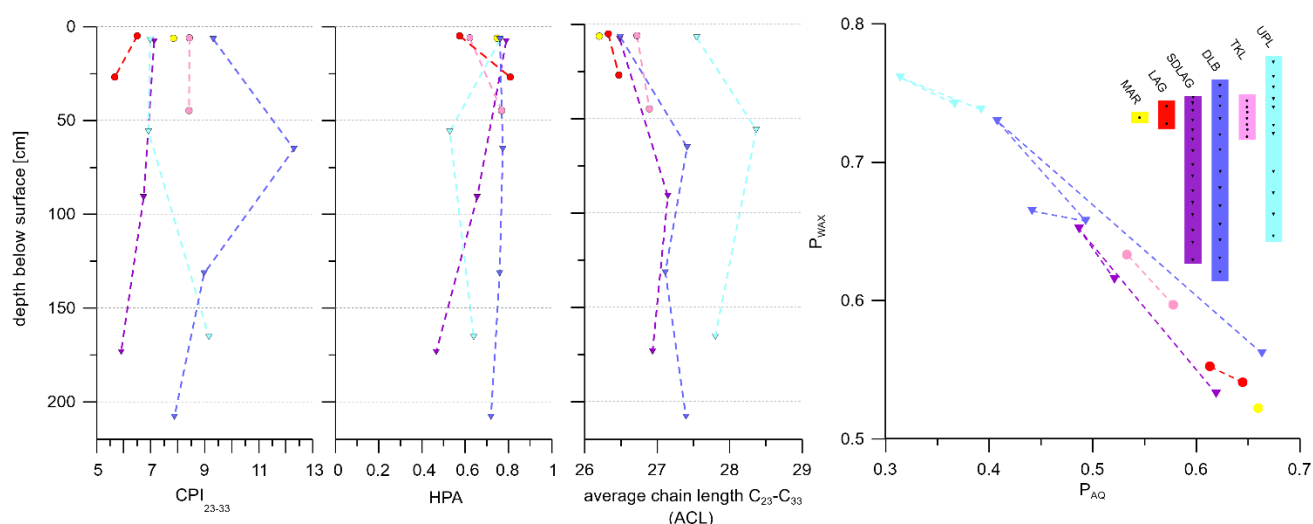
Figure 4: Plots of the organic carbon quality and sources, indicated by the lipid-biomarker indices carbon preference index (CPI), higher plant index (HPA), average chain length (ACL) and the proxies P_{AQ}, for aquatic OM, and P_{WAX}, for terrestrial OM, with circles representing unfrozen sediments and triangles representing frozen sediments. Core abbreviations: UPL: upland permafrost; TKL: thermokarst lake; DLB: drained lake basin; SDLAG: semi-drained lagoon; LAG: lagoon; MAR: marine.

4.3.2 Organic carbon quality-indicating indices

The carbon preference index of *n*-alkanes (CPI) shows the widest range in the samples of the DLB core, ranging between 7.88 in the deepest sample and the overall highest value of 12.31, calculated for the sample from a depth of 65.25 cm b.s.l. (figure 4). The lowest CPI values of 5.67 and 6.51 were measured in the LAG samples (figure 4).

The higher plant index (HPA) varies between 0.46 in the deepest SDLAG sample, and 0.81 in the deeper LAG sample (figure 4). The patterns of the HPA over depths in UPL, DLB and SDLAG samples are similar to the pattern of the CPI in terms of values increasing or decreasing over depth within each site (figure 4). In contrast, the patterns of the HPA over depth of TKL and LAG are reversed compared to the CPI, with an increasing value from the deeper sample to the uppermost one (figure 4). The dataset is available at Giest et al. (2024c).

9

5 Discussion

5.1 Organic carbon

5.1.1 Carbon stocks under various geomorphological influences

The total range of TOC contents, as well as the TOCvol, of all samples is wide (TOC: 0.72–37.62 wt%; TOCvol: 6.79–119.7 kg m^{-3}) (figures 3 & S3), but comparable to other studies that include permafrost and thermokarst features (TOC: 0.2–43 wt%; TOCvol: 2.8–93.5 kg m^{-3}) (Strauss et al., 2015;Schirrmeister et al., 2011;Fuchs et al., 2018). A reason for this variability is probably the heterogeneity of the organic source material from the different permafrost and thermokarst landscape features including well-preserved peat, paleosoils and marine influenced coastal areas. The large range of the TOC content (2.94–37.62 wt%) in the DLB core is likely caused by such a mixture of permafrost soils and thermokarst lake origin with different material type input and decomposition processes. Additionally, post-drainage peat accumulation that caused the high TOC contents in the upper soil of the DLB, has been previously shown in other drained thermokarst lake basin studies as well (Fuchs et al., 2019; Jones et al., 2012; Lenz et al., 2016). The large, often flat-bottomed drained lake basins provide perfect conditions for the formation of wetlands, through which most become vegetated in 5–10 years after the drainage event and accumulate peat 10–20 years after (Bockheim et al., 2004; Jones et al., 2012). Compared to the mean TOCvol of permafrost deposits from the Yedoma region (19 kg m^{-3}) and of thermokarst deposits (33 kg m^{-3}) (Strauss et al., 2013), the mean TOCvol of the cores of this study are relatively high (UPL: 37 kg m^{-3}; TKL: 48 kg m^{-3}; DLB: 25 kg m^{-3}; SDLAG: 32 kg m^{-3}), revealing a large pool of carbon in all deposits studied (figure S3). The high TOCvol in the TKL deposits, significantly higher than in the SDLAG and DLB deposits, are likely the result of an interplay of various factors. It might be partially related to the relocation of organic matter (OM) e.g., due to erosion, leading to OC accumulation in the basin and thaw subsidence progression due to ground ice loss (Lenz et al., 2016). Additionally, it is likely that there is a higher input of Holocene OC and an increased primary productivity in the lake stimulated by nutrient release from thawing permafrost (Strauss et al., 2015;Strauss et al., 2024;Wolter et al., 2018). The accumulation of OC might be further accelerated by slow decomposition rates in the cold and anaerobic lake environment (Strauss et al., 2015;Haugk et al., 2022;Jongejans et al., 2018). The lower TOCvol in the refrozen thermokarst features (SDLAG & DLB) might partially be influenced by ground ice accumulation after the drainage of the water bodies. In case of the SDLAG deposits, the lower TOCvol is combined with a low mean TOC content (2.37 wt%), which might be also influenced by a decrease of the primary productivity with the transition from thermokarst lake to lagoon, since strong seasonal fluctuations of the salt content, the lowered, fluctuating water level to almost drainage, and the bedfast ice formation in winter, shortens the period of biological production. Moreover, there might have been decomposition of OM in the SDLAG deposits all year round when the lagoon had more water or rather was in the state of a thermokarst lake, which also could have led to a decreased TOC content.

5.1.2 Influence of various OM sources

The analysis of the OC and lipid biomarkers in the deposits shows that they contain OM from different sources, likely additionally influenced by parameters such as salinity, temperature, and water availability. This results in two end members for the sample set, MAR and UPL, with the other sites aligning between. It nicely depicts the transformation processes of soil OM over the course of landscape development from dry terrestrial permafrost over thermokarst lakes, saltwater exposure and finally a marine state (Jenrich et al., 2021). One indicator for the source of OM is the TOC/TN ratio, with lower values indicating a stronger aquatic influence and higher values indicating a stronger terrestrial influence (Meyers, 1997). The highest mean TOC/TN ratio was measured in the UPL deposits (17.2), significantly higher than in the three thermokarst landscape features included in the statistical analysis, indicating the strongest terrestrial influence on the OM composition of the UPL core (figure 3 & S3). The lowest mean TOC/TN ratios, significantly lower than in the UPL and TKL deposits, were measured in the LAG and SDLAG samples (13.1), indicating the strongest aquatic influence on those deposits, e.g. from algae and

343 bacteria. The largest variation of the TOC/TN ratio is shown in the DLB core (11.7–58.5), indicating different sources of OM

344 during the different stages of the thermokarst lake evolution. Since the TOC/TN ratio can also be influenced by other processes

345 like the level of degradation of OM, we also analysed the *n*-alkane distribution in the samples and calculated the P_{aq} and P_{wax}

346 as indicators of the source of OM. The results of these parameters also show the two end members (figure 4) with the highest

347 ACL values and highest P_{wax}, thus the strongest terrestrial influence on the OM composition in the UPL deposits and the

348 strongest aquatic influence on the OM composition in the marine sample, with the lowest ACL and a high P_{aq}. It is also shown

349 in figure 4 that all thermokarst deposits (LAG, SDLAG, DLB & TKL) align between the two end members, thus are stronger

350 influenced by aquatic OM than the UPL samples. Moreover, figure 4 hints on a change of source of OM in the SDLAG, DLB

351 and UPL profiles from the upper soil compared to the samples between 50 and 100 cm b.s.l. and between 100 and 200 cm

352 b.s.l. This might not be influenced by different stages of the thermokarst lake evolution, but rather by changes of hydrological

353 conditions at the time of deposition, or by the relocation of OM, for example due to cryoturbation or roots, since both the

354 terrestrial endmember UPL and the thermokarst features show that changes.

5.1.3 Organic carbon degradation

356 The decomposition of OM releases carbon as CO_2 and CH_4 and portions of nitrogen as N_2O from the soils to the atmosphere

357 (Schuur et al., 2022; Strauss et al., 2024; Voigt et al., 2020). Deposits containing further degraded OM have lower TOC/TN

358 ratios than those containing fresh OM due to a larger share of nitrogen in the soils (Andersson et al., 2012; Weintraub and

359 Schimel, 2005). Thus, in addition to the OM sources the TOC/TN ratios also contain a component dependent on the OM

360 decomposition level. As seen above, the TOC/TN ratios in the UPL deposits were significantly higher compared to the

361 thermokarst influenced deposits (SDLAG, TKL, DLB), which was interpreted as a higher terrestrial character of the OM in

362 the UPL samples. However, these differences are likely also influenced by OM degradation during unfrozen periods of the

363 thermokarst deposits. The mean TOC/TN ratio of UPL is lower than in comparable sites (Routh et al. 2014, Fuchs et al. 2019),

364 while TKL and DLB show higher values, indicating a relatively high level of preservation of the accumulated OM, leading to

365 a likely high quality for future degradation and therefore a vulnerability to decomposition after thaw.

366 The carbon isotopic signal is also influenced by both factors: OM sources and OM degradation. Terrestrial material usually

367 shows lighter and marine OM heavier $\delta^{13}C$ signals and due to the preferred release of $^{12}CO_2$ during degradation, the residual

368 OM becomes isotopically heavier (Andersson et al., 2012). In the uppermost samples (down to 50 cm) the data resembled the

369 two-end member model of the OM sources with the UPL samples showing the lightest $\delta^{13}C$ values (stronger terrestrial

370 character) and the MAR sample exhibiting the heaviest signal (marine influenced) (figure 3). The other samples show

371 intermediate data resembling supply of different OM sources and/or different level of degradation. In the deeper part the picture

372 is less clear. The UPL samples are isotopically heavier plotting in the range of the DLB data, whose $\delta^{13}C$ signal is relatively

373 constant throughout the whole core. This could indicate a higher level of degradation of OM in the deeper UPL deposits. The

374 deeper SDLAG samples are, with exception of the deepest sample, isotopically significantly heavier which could indicate a

375 stronger aquatic/marine influence in the lagoon during time of deposition rather than a stronger degradation of the OM.

376 Also, the CPI depends on both the source of OM and the level of OM maturation. The original odd-over even carbon number

377 predominance of the indigenous *n*-alkanes in a sample is determined by the source material and is changing to lower values

378 during OM maturation. Here, the wide range of different CPIs most likely rather resemble the various mixtures of OM at the

379 different sites. This is supported by findings of Jongejans et al. (2021), also reporting that the CPI represents rather the source

380 OM in such relatively young sediments. The HPA shows a very narrow band of values for all samples. In the uppermost sample

381 of the TKL and LAG, samples show a shift to lower values which could indicate a higher degradation of the OM in the surface

382 sediments. The UPL and SDLAG samples show lower HPA values in the deeper part of the core which might point to periods

383 of stronger degradation in the past. However, the material shows low variability in the HPA values overall, plotting in the

384 upper scale of the parameter and therefore indicating relatively less degraded OM. Thus, with ongoing climate warming and

385 thawing of the deeper permafrost layers, the preserved OM of good quality could become available to decomposition, leading
386 to increased emissions of greenhouse gases.

**5.2 Effects of OC characteristics on environmental mercury**

Processes that have an influence on OC characteristics in soils can also have effects on further parameters, a prominent one being THg. To identify such associations, a correlation matrix was computed integrating the measured biogeochemical and sedimentological parameters (figure 5). TOC content and TOCvol are weakly positively correlated with the Hg content in the samples (correlation factor 0.34 and 0.42, respectively). In general, sources for Hg, accumulating in Arctic soils, can be both natural and anthropogenic. Natural sources, contributing to the increase of atmospheric Hg and subsequent deposition into soils, include boreal forest fires and volcanic activity. Anthropogenic input has significantly intensified due to industrialization and expanding land use (Jonsson et al., 2017). A reason for the positive correlation of the TOCvol with Hg is presumably that approximately 70 % of the Hg in the Arctic tundra is derived from gaseous elemental Hg, which is ubiquitously present in the atmosphere (Obrist et al., 2017). Since the deposition of gaseous elemental Hg is strongly influenced by the Hg uptake of vegetation, sites with a higher input of OM and therefore higher TOCvol also accumulate higher levels of Hg bound in the plant matter (Obrist et al., 2017). The Hg content in the deposits is furthermore negatively correlated with the δ^{13}C ratio (-0.42), which we found to be very weak, like for TOC. This correlation indicates that there are higher mercury contents in the deposits with OM from a terrestrial or mixed terrestrial/aquatic source. For example, the marine influenced MAR sample with the highest δ^{13}C signal shows the lowest HG content and the upper UPL samples with the lower δ^{13}C signal shows higher HG contents than the lower UPL samples with the higher δ^{13}C signal (figure 3). The same can be observed for the SDLAG samples. Mainly, the Hg content correlates negatively with the mean grain size (-0.77). This is displayed in the mercury contents in the fine-grained freshwater thermokarst features (mean DLB: 69.87 µg kg^{-1}; mean TKL: 70.74 µg kg^{-1}) that are significantly higher than in the UPL deposits (mean UPL: 40.16 µg kg^{-1}). A reason for this could be that the thermokarst processes might affect the distribution and accumulation of Hg due to the release of Hg from previously freeze-looked Hg-containing OM in the soil upon decomposition (Schuster et al., 2018). Additionally, thermokarst, erosion and an increased soil water movement in a thickening active layer, all triggered by permafrost thaw, can increase the transport of Hg from the soils to Arctic surface waters, resulting in higher Hg concentrations in lacustrine and post-drainage sediments (Rydberg et al., 2010), which is also indicated by the data of this study. Especially in the SDLAG core the correlation of thermokarst processes with OC and sediment characteristics and the Hg content is visible. The GSD shows a peak at coarser grain sizes, between fine sand and silt, similar to the UPL deposits in the deeper half of the core below 100 cm b.s.l. (figure 2). The upper half of the core shows a peak at finer grain sizes similar to the thermokarst features, indicating lacustrine deposits (figure 2). This shift indicates that there is less influence of thermokarst processes in the deeper half of the core. Additionally, there are lower Hg contents in the deeper part (15.57–48.65 µg kg^{-1}) akin to the Hg content in the UPL deposits and accompanied by low TOC contents (0.74–1.35 wt%) (figure 3). In contrast, the thermokarst influenced upper half of the core show higher Hg concentrations (20.27–102.17 µg kg^{-1}), similar to the Hg concentrations in the other thermokarst features, accompanied by higher TOC contents (0.72–4.65 wt%) (figure 3).
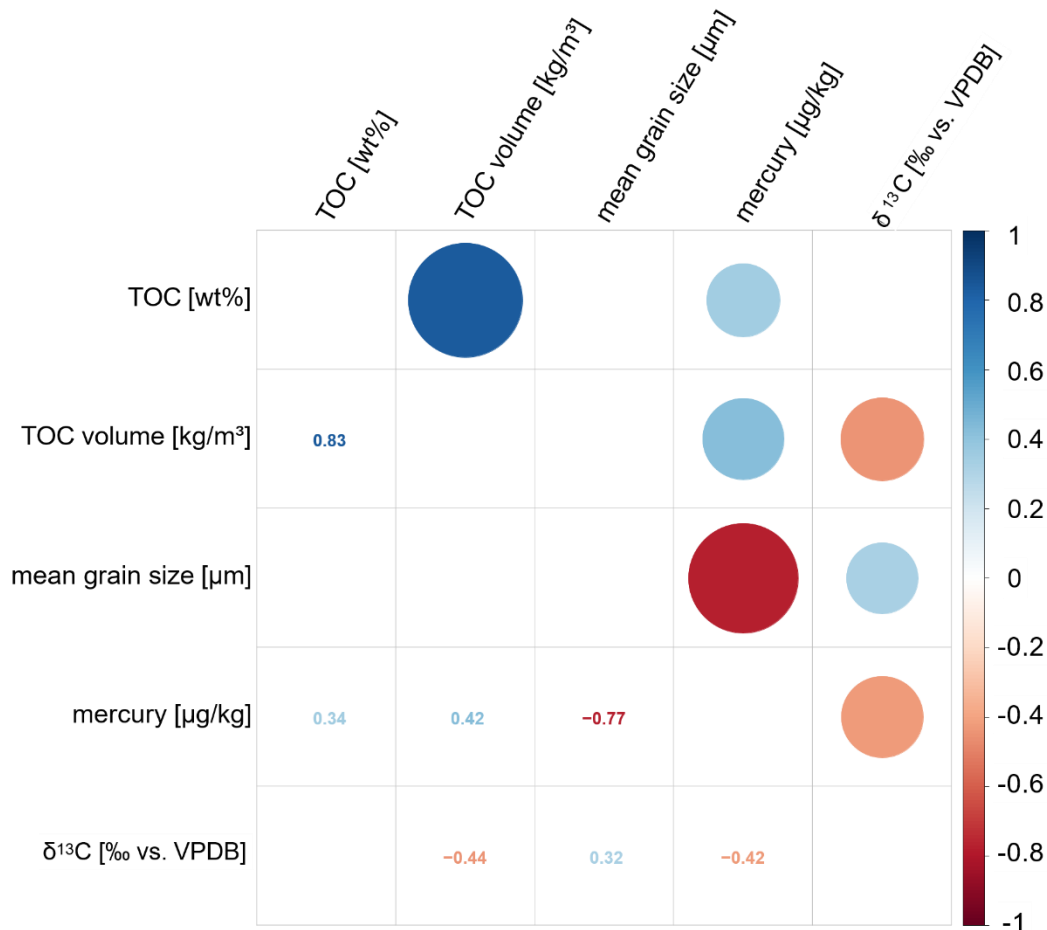
Figure 5: Correlation matrix of sedimentological and biogeochemical parameters. Strong positive correlations in dark blue, strong negative correlations in dark red. TOC: total organic carbon content in weight percent; TOC volume: organic carbon density; $\delta^{13}C$: stable carbon isotope ratio in per mil relative to Vienna PeeDee Belemnite standard.

**5.3 Influence of salinity and soil condition on the biogeochemical soil characteristics**

Looking at the differences in ACL and $\delta^{13}C$, specifically comparing saline, unfrozen deposits with non-saline, frozen deposits, and combining it with the rather low TOC/TN ratios in the saline deposits, which is typical for aquatic OM, it is evident that the saline deposits examined in this study showcase a stronger aquatic influence in their OM composition. The CPI values are higher in the non-saline samples, which could resemble different odd over even carbon number predominance distribution of *n*-alkanes in the aquatic/marine vs. terrestrial organic biomass. All three parameters, the $\delta^{13}C$, the TOC/TN ratio, and the CPI, might additionally indicate more fresh, undegraded OM in the non-saline deposits, which is likely influenced by a decreased input of fresh OM in the saline environments due to a decreased primary productivity, an increased microbial activity, since the salinity in the soil water leads to a depression of its freezing point, thus a longer unfrozen period, and less retention of fresh OM in the coarse marine sediments (Bischoff et al., 2018; Jongejans, 2022).
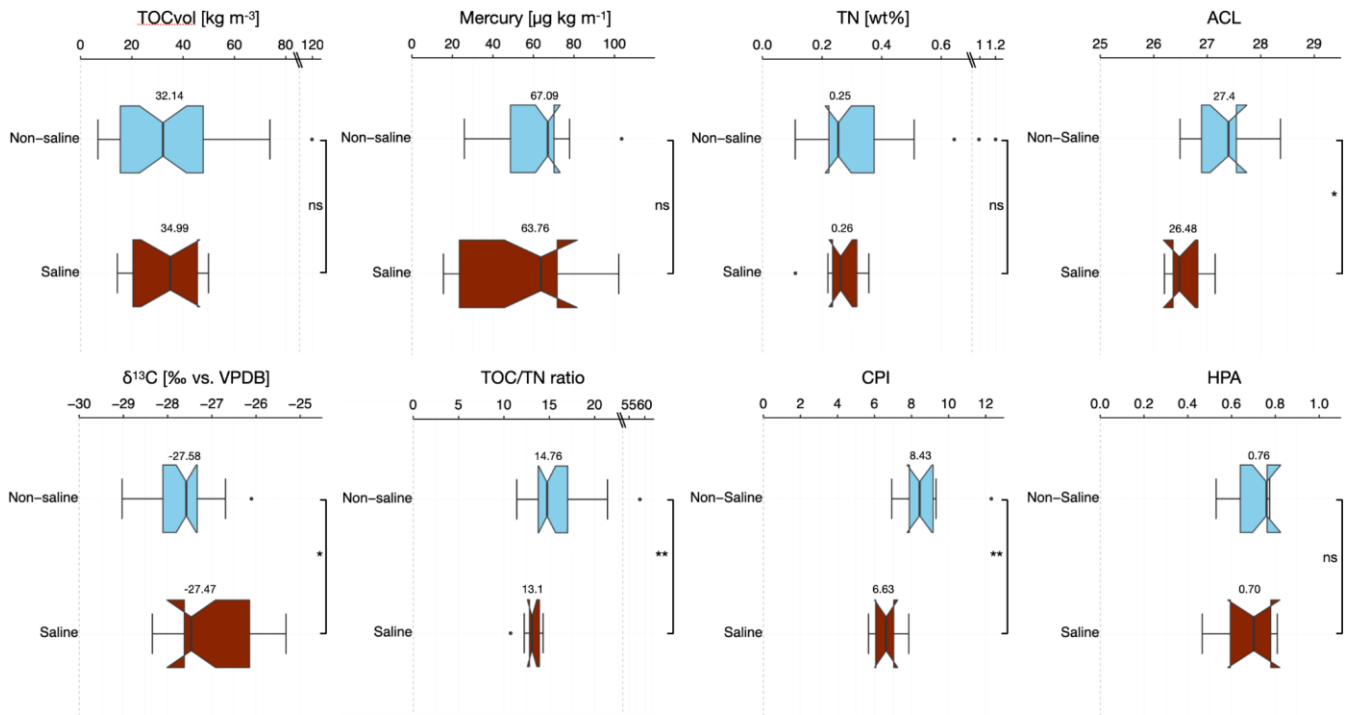
Figure 6: Boxplots of the biogeochemical parameters divided in saline and non-saline sediments: total organic carbon density (TOCvol) [$kg_{TOC} m^{-3}$], Mercury [$\mu g\ kg^{-1}$], total nitrogen (TN) in weight percent [wt%], average chain length of *n*-alkanes (ACL), stable carbon isotope ratio ($\delta^{13}C$) per mil relative to Vienna PeeDee Belemnite standard [‰ vs. VPDB], total organic carbon/total nitrogen ratio (TOC/TN ratio), carbon preference index (CPI), and higher plant alcohol index (HPA) of profiles in non-saline [blue] (including upland permafrost, thermokarst lake sediments, and drained lake basin sediments) and saline [red] (including semi-drained lagoon sediments, lagoon sediments, and marine sediments) soil settings. The whiskers display the data range (outliers as black points), and the boxes show the interquartile range (25–75 %). The black vertical line marks the median and the notches represent the 95 % confidence interval. The bars right of the boxes show the statistical significance of differences between the groups (ns = not significant; * = $p < 0.05$; ** = $p < 0.01$; *** = $p < 0.001$).

Moreover, the comparison of the frozen and unfrozen deposits shows significant differences in the TOCvol and the TN content. The frozen deposits have significantly lower TOCvol (median 24 kg m^{-3}) and TN (median 0.24 wt%) compared to the unfrozen deposits (median TOCvol 48.41 kg m^{-3}; median TN 0.36 wt%) (figure 7). The higher TN content in the unfrozen deposits is likely influenced by erosion processes, reactivated soil water movement in thawed permafrost, as well as surface runoff from nitrogen-rich upland permafrost and the refrozen thermokarst features, leading to the deposition of nitrogen in the aquatic systems (Strauss et al., 2024). Furthermore, if bioavailable, the increased TN content in thawed permafrost soils could potentially enhance the ecosystem productivity (Strauss et al., 2022), thereby influencing the increased TOCvol in the unfrozen deposits. Also, the significantly lower $\delta^{13}C$ values in the unfrozen deposits potentially indicates a higher input of fresh OM to the unfrozen thermokarst environments. Additionally, thaw subsidence progression in the unfrozen deposits and the accumulation of ground ice in the (re)frozen deposits likely have an influence on the TOCvol (Strauss et al., 2015).
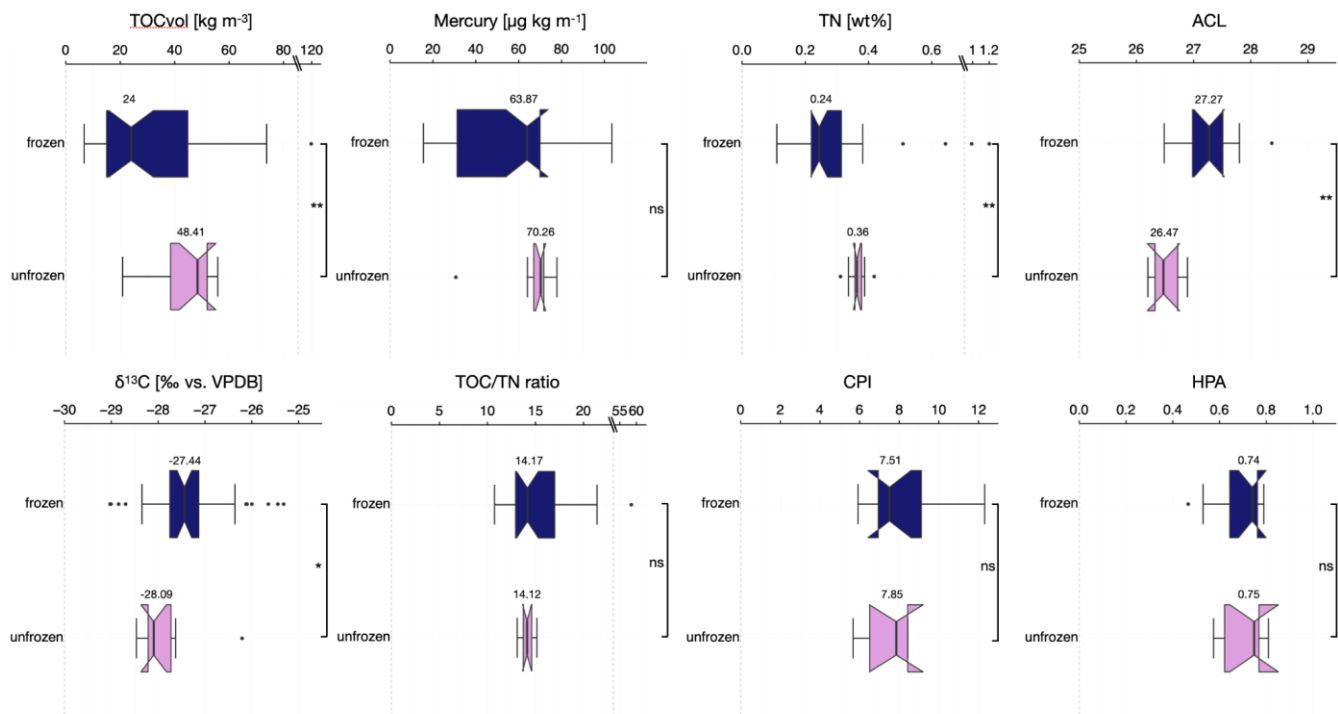
Figure 7: Boxplots of the biogeochemical parameters divided in frozen and unfrozen sediments: total organic carbon density (TOCvol) [$kg_{TOC}m^{-3}$], Mercury [µg kg⁻¹], total nitrogen (TN) in weight percent [wt%], average chain length of *n*-alkanes (ACL), stable carbon isotope ratio ($\delta^{13}C$) per mil relative to Vienna PeeDee Belemnite standard [‰ vs. VPDB], total organic carbon/total nitrogen ratio (TOC/TN ratio), carbon preference index (CPI), and higher plant alcohol index (HPA) of frozen profiles [dark blue] (including upland permafrost, drained lake basin sediments, and semi-drained lagoon sediments) and unfrozen [pink] (including thermokarst lake sediments, lagoon sediments, and marine sediments) soil profiles. The whiskers display the data range (outliers as black points), and the boxes show the interquartile range (25–75 %). The black vertical line marks the median and the notches represent the 95 % confidence interval. The bars right of the boxes show the statistical significance of differences between the groups (ns = not significant; * = $p < 0.05$; ** = $p < 0.01$; *** = $p < 0.001$).

The HPA data are quite similar for the frozen/unfrozen and saline/non-saline sites and plot in the upper range of the parameter scale. This could indicate a comparable level of degradation between all sites and the potential to act as a good substrate for greenhouse gas production when actively metabolized. No significant differences were additionally identified for the Hg content. This might be influenced by the way Hg accumulates in sedimentary deposits. We see evidence that thawing permafrost initiates the reactivation and accumulation of Hg in thermokarst affected deposits. Unlike other measured parameters, these processes are not necessarily reversed upon refreezing of the deposits, but instead tend to pause until repeated thawing of the soils. Consequently, the amount of Hg in the soils is likely to increase with every thermokarst lake and thawing cycle the deposits undergo, without the current soil condition and other properties such as salinity, having a major influence accumulative effect.

6 Conclusion

The analysis of the six sediment cores from a thermokarst-affected coastal lowland in North Alaska showed that the OC characteristics in deposits of the different landscape features are diverse. The highest TOC contents were measured in the drained lake basin and thermokarst lake deposits, likely caused by an increased primary productivity and Holocene OC input. This is also reflected by the analysis of the quality of OC, with high CPI values indicating fresh, undegraded OM in both profiles. The deposits of a semi-drained thermokarst lagoon had significantly lower TOC contents than the freshwater-influenced thermokarst deposits. Additionally, there were significant differences in the CPI, $\delta^{13}C$, and TOC/TN ratio between saline and non-saline deposits, indicating a domination of aquatic OM in the saline deposits, and moreover likely indicating a higher level of fresh, undegraded OM in the non-saline deposits. The intrusion of saltwater to the deposits seems to lead to a lower quality of OM in the soils, likely influenced by a lower input of fresh OM due to a decreased primary productivity, and

potentially enhanced by degradational processes. Indicated by the ACL and P_{aq}, P_{wax}, all thermokarst-influenced deposits showed a stronger aquatic influence on the OM composition than the upland permafrost deposits. Besides the differences in the source of OM, the comparison of unfrozen and frozen deposits showed higher TOCvol and TN contents in the unfrozen deposits. This is also likely influenced by differences in the level of primary productivity, depositional- and degradational processes. Concerning mercury, this study demonstrates that the characteristics of carbon in Arctic soils significantly influence the distribution and accumulation of mercury, with variations likely driven by natural sources as well as sedimentological and thermokarst processes. Weak positive correlations between TOC content and Hg suggest a link between organic matter inputs and Hg deposition, while strong negative correlations with grain size highlight the enrichment of Hg in fine-grained deposits associated with thermokarst dynamics. Thus, our findings provide valuable insights into the dynamics of carbon storage and vulnerability to decomposition in response to environmental changes in a coastal permafrost landscape, since they reflect the complex interplay of environmental factors, landform characteristics and impacts of climate change on these dynamic Arctic landscapes. The integration of carbon dioxide and methane emission measurements in further studies could complement the findings and provide an even more comprehensive picture of carbon fluxes across the geomorphological, hydrological, and ecological diverse landscapes of Arctic coastal lowlands and the influence of permafrost thaw and saltwater intrusion on the deposits.

Data availability. The data used in this manuscript are available online: Biomarkers of sediment cores from a land – shore transect in the Teshekpuk Lake Region in Arctic Alaska, 2022 (Giest et al. (2024c), https://doi.org/10.1594/PANGAEA.971595); Sedimentological characteristics of sediment cores from a land – shore transect in the Teshekpuk Lake Region in Arctic Alaska, 2022 (Giest et al. (2024a), https://doi.org/10.1594/PANGAEA.971244); Biogeochemical characteristics of sediment cores from a land – shore transect in the Teshekpuk Lake Region in Arctic Alaska, 2022 (Giest et al. (2024b), https://doi.org/10.1594/PANGAEA.971246).

Supplement. The supplement related to this article will be available online.

Competing interests. The authors declare that nobody of the author team has any competing interests.

Author contributions. J. Strauss, M. Jenrich and F. Giest designed this study. J. Strauss, G. Grosse, and M. Jenrich developed the overall coring plans for the Perma-X Lagoons field campaign and conducted the fieldwork in 2022. B. M. Jones provided guidance on site selection, field assistance, and logistical support for the expedition. J. Strauss, M. Jenrich and F. Giest did the subsampling for all cores. F. Giest carried out the laboratory analyses. K. Mangelsdorf supported the biomarker interpretation. F. Giest wrote the first draft of the manuscript. All co-authors contributed within their specific expertise to data interpretation as well as manuscript writing.

References

Andersson, R. A., Meyers, P., Hornibrook, E., Kuhry, P., and Mörth, C.: Elemental and isotopic carbon and nitrogen records of organic matter accumulation in a Holocene permafrost peat sequence in the East European Russian Arctic, J Quaternary Science, 27, 545–552, https://doi.org/10.1002/jqs.2541, 2012.

Arp, C. D., Jones, B. M., Urban, F. E., and Grosse, G.: Hydrogeomorphic processes of thermokarst lakes with grounded-ice and floating-ice regimes on the Arctic coastal plain, Alaska, Hydrological Processes, 25, 2422–2438, https://doi.org/10.1002/hyp.8019, 2011.

Ballinger, T. J., Bigaalke, S., Walsh, J. E., Brettschneider, B., Thoman, R. L., Bhatt, U. S., Hanna, E., Hanssen-Bauer, I., Kim, S.-J., Overland, J. E., and Wang, M.: NOAA Arctic Report Card 2023: Surface Air Temperature, https://doi.org/10.25923/X3TA-6E63, 2023.

Bischoff, N., Mikutta, R., Shibistova, O., Dohrmann, R., Herdtle, D., Gerhard, L., Fritzsche, F., Puzanov, A., Silanteva, M., Grebennikova, A., and Guggenberger, G.: Organic matter dynamics along a salinity gradient in Siberian steppe soils, Biogeosciences, 15, 13–29, https://doi.org/10.5194/bg-15-13-2018, 2018.

Biskaborn, B. K., Smith, S. L., Noetzli, J., Matthes, H., Vieira, G., Streletskiy, D. A., Schoeneich, P., Romanovsky, V. E., Lewkowicz, A. G., Abramov, A., Allard, M., Boike, J., Cable, W. L., Christiansen, H. H., Delaloye, R., Diekmann, B., Drozdov, D., Etzelmüller, B., Grosse, G., Guglielmin, M., Ingeman-Nielsen, T., Isaksen, K., Ishikawa, M., Johansson, M., Johannsson, H., Joo, A., Kaverin, D., Kholodov, A., Konstantinov, P., Kröger, T., Lambiel, C., Lanckman, J.-P., Luo, D., Malkova, G., Meiklejohn, I., Moskalenko, N., Oliva, M., Phillips, M., Ramos, M., Sannel, A. B. K., Sergeev, D., Seybold, C., Skryabin, P., Vasiliev, A., Wu, Q., Yoshikawa, K., Zheleznyak, M., and Lantuit, H.: Permafrost is warming at a global scale, Nat Commun, 10, 264, https://doi.org/10.1038/s41467-018-08240-4, 2019.

Blott, S. J. and Pye, K.: GRADISTAT: a grain size distribution and statistics package for the analysis of unconsolidated sediments, Earth Surf Processes Landf, 26, 1237–1248, https://doi.org/10.1002/esp.261, 2001.

Bockheim, J. G., Hinkel, K. M., Eisner, W. R., and Dai, X. Y.: Carbon Pools and Accumulation Rates in an Age-Series of Soils in Drained Thaw-Lake Basins, Arctic Alaska, Soil Science Soc of Amer J, 68, 697–704, https://doi.org/10.2136/sssaj2004.6970, 2004.

Bray, E. E. and Evans, E. D.: Distribution of n-paraffins as a clue to recognition of source beds, Geochimica et Cosmochimica Acta, 22, 2–15, https://doi.org/10.1016/0016-7037(61)90069-2, 1961.

Cohen, J., Zhang, X., Francis, J., Jung, T., Kwok, R., Overland, J., Ballinger, T. J., Bhatt, U. S., Chen, H. W., Coumou, D., Feldstein, S., Gu, H., Handorf, D., Henderson, G., Ionita, M., Kretschmer, M., Laliberte, F., Lee, S., Linderholm, H. W., Maslowski, W., Peings, Y., Pfeiffer, K., Rigor, I., Semmler, T., Stroeve, J., Taylor, P. C., Vavrus, S., Vihma, T., Wang, S., Wendisch, M., Wu, Y., and Yoon, J.: Divergent consensuses on Arctic amplification influence on midlatitude severe winter weather, Nat. Clim. Chang., 10, 20–29, https://doi.org/10.1038/s41558-019-0662-y, 2020.

Ficken, K. J., Li, B., Swain, D. L., and Eglinton, G.: An n-alkane proxy for the sedimentary input of submerged/floating freshwater aquatic macrophytes, Organic Geochemistry, 31, 745–749, https://doi.org/10.1016/S0146-6380(00)00081-4, 2000.

Fuchs, M., Grosse, G., Strauss, J., Gunther, F., Grigoriev, M., Maximov, G. M., and Hugelius, G.: Carbon and nitrogen pools in thermokarst-affected permafrost landscapes in Arctic Siberia, Biogeosciences, 15, 953-971, doi:10.5194/bg-15-953-2018, 2018.

Fuchs, M., Lenz, J., Jock, S., Nitze, I., Jones, B. M., Strauss, J., Günther, F., and Grosse, G.: Organic Carbon and Nitrogen Stocks Along a Thermokarst Lake Sequence in Arctic Alaska, JGR Biogeosciences, 124, 1230–1247, https://doi.org/10.1029/2018JG004591, 2019.

Giest, F., Jenrich, M., Grosse, G., Jones, B., Mangelsdorf, K., Windirsch, T., and Strauss, J.: Sedimentological characteristics of sediment cores from a land – shore transect in the Teshekpuk Lake Region in Arctic Alaska, 2022. PANGAEA, 2024a.

Giest, F., Jenrich, M., Grosse, G., Jones, B., Mangelsdorf, K., Windirsch, T., and Strauss, J.: Biogeochemical characteristics of sediment cores from a land – shore transect in the Teshekpuk Lake Region in Arctic Alaska, 2022. PANGAEA, 2024b.

Giest, F., Jenrich, M., Grosse, G., Jones, B., Mangelsdorf, K., Windirsch, T., and Strauss, J.: Biomarkers of sediment cores from a land – shore transect in the Teshekpuk Lake Region in Arctic Alaska, 2022. PANGAEA, 2024c.

Grosse, G., Jones, B., and Arp, C.: 8.21 Thermokarst Lakes, Drainage, and Drained Basins, in: Treatise on Geomorphology, Elsevier, 325–353, https://doi.org/10.1016/B978-0-12-374739-6.00216-5, 2013.

Haugk, C., Jongejans, L. L., Mangelsdorf, K., Fuchs, M., Ogneva, O., Palmtag, J., Mollenhauer, G., Mann, P. J., Overduin, P. P., Grosse, G., Sanders, T., Tuerena, R. E., Schirrmeister, L., Wetterich, S., Kizyakov, A., Karger, C., and Strauss, J.: Organic matter characteristics of a rapidly eroding permafrost cliff in NE Siberia (Lena Delta, Laptev Sea region), Biogeosciences, 19, 2079-2094, doi:10.5194/bg-19-2079-2022, 2022.

Hugelius, G., Strauss, J., Zubrzycki, S., Harden, J. W., Schuur, E. A. G., Ping, C.-L., Schirrmeister, L., Grosse, G., Michaelson, G. J., Koven, C. D., O'Donnell, J. A., Elberling, B., Mishra, U., Camill, P., Yu, Z., Palmtag, J., and Kuhry, P.: Estimated stocks of circumpolar permafrost carbon with quantified uncertainty ranges and identified data gaps, Biogeosciences, 11, 6573–6593, https://doi.org/10.5194/bg-11-6573-2014, 2014.

Intergovernmental Panel on Climate Change (IPCC): The Ocean and Cryosphere in a Changing Climate: Special Report of the Intergovernmental Panel on Climate Change, 1st ed., Cambridge University Press, https://doi.org/10.1017/9781009157964, 2022.

Intergovernmental Panel on Climate Change (IPCC): Climate Change 2022 – Impacts, Adaptation and Vulnerability: Working Group II Contribution to the Sixth Assessment Report of the Intergovernmental Panel on Climate Change, 1st ed., Cambridge University Press, https://doi.org/10.1017/9781009325844, 2023.

Jenrich, M., Angelopoulos, M., Grosse, G., Overduin, P. P., Schirrmeister, L., Nitze, I., Biskaborn, B. K., Liebner, S., Grigoriev, M., Murray, A., Jongejans, L. L., and Strauss, J.: Thermokarst Lagoons: A Core-Based Assessment of Depositional Characteristics and an Estimate of Carbon Pools on the Bykovsky Peninsula, Front. Earth Sci., 9, 637899, https://doi.org/10.3389/feart.2021.637899, 2021.

Jones, B. M. and Arp, C. D.: Observing a Catastrophic Thermokarst Lake Drainage in Northern Alaska, Permafrost & Periglacial, 26, 119–128, https://doi.org/10.1002/ppp.1842, 2015.

Jones, B. M., Arp, C. D., Jorgenson, M. T., Hinkel, K. M., Schmutz, J. A., and Flint, P. L.: Increase in the rate and uniformity of coastline erosion in Arctic Alaska, Geophysical Research Letters, 36, 2008GL036205, https://doi.org/10.1029/2008GL036205, 2009.

Jones, B. M., Farquharson, L. M., Baughman, C. A., Buzard, R. M., Arp, C. D., Grosse, G., Bull, D. L., Günther, F., Nitze, I., Urban, F., Kasper, J. L., Frederick, J. M., Thomas, M., Jones, C., Mota, A., Dallimore, S., Tweedie, C., Maio, C., Mann, D. H., Richmond, B., Gibbs, A., Xiao, M., Sachs, T., Iwahana, G., Kanevskiy, M., and Romanovsky, V. E.: A decade of remotely sensed observations highlight complex processes linked to coastal permafrost bluff erosion in the Arctic, Environ. Res. Lett., 13, 115001, https://doi.org/10.1088/1748-9326/aae471, 2018.

Jones, B. M., Grosse, G., Farquharson, L. M., Roy-Léveillée, P., Veremeeva, A., Kanevskiy, M. Z., Gaglioti, B. V., Breen, A. L., Parsekian, A. D., Ulrich, M., and Hinkel, K. M.: Lake and drained lake basin systems in lowland permafrost regions, Nat Rev Earth Environ, 3, 85–98, https://doi.org/10.1038/s43017-021-00238-9, 2022.

Jones, M. C., Grosse, G., Jones, B. M., and Walter Anthony, K.: Peat accumulation in drained thermokarst lake basins in continuous, ice-rich permafrost, northern Seward Peninsula, Alaska, J. Geophys. Res., 117, 2011JG001766, https://doi.org/10.1029/2011JG001766, 2012.

Jongejans, L. L., Strauss, J., Lenz, J., Peterse, F., Mangelsdorf, K., Fuchs, M., and Grosse, G.: Organic matter characteristics in yedoma and thermokarst deposits on Baldwin Peninsula, west Alaska, Biogeosciences, 15, 6033-6048, doi:10.5194/bg-15-6033-2018, 2018.

Jongejans, L. L.: Ablagerung von organischem Kohlenstoff in eisreichem PermafrostOrganic matter stored in ice-rich permafrost: future permafrost thaw and greenhouse gas release: zukünftige Permafrosttauen und Treibhausgasemissionen, Universität Potsdam, https://doi.org/10.25932/PUBLISHUP-56491, 2022.

Jongejans, L. L., Mangelsdorf, K., Schirrmeister, L., Grigoriev, M. N., Maksimov, G. M., Biskaborn, B. K., Grosse, G., and Strauss, J.: n-Alkane Characteristics of Thawed Permafrost Deposits Below a Thermokarst Lake on Bykovsky Peninsula, Northeastern Siberia, Front. Environ. Sci., 8, 118, https://doi.org/10.3389/fenvs.2020.00118, 2020.

Jongejans, L. L., Liebner, S., Knoblauch, C., Mangelsdorf, K., Ulrich, M., Grosse, G., Tanski, G., Fedorov, A. N., Konstantinov, P. Ya., Windirsch, T., Wiedmann, J., and Strauss, J.: Greenhouse gas production and lipid biomarker distribution in Yedoma and Alas thermokarst lake sediments in Eastern Siberia, Global Change Biology, 27, 2822–2839, https://doi.org/10.1111/gcb.15566, 2021.

Jonsson, S., Andersson, A., Nilsson, M. B., Skyllberg, U., Lundberg, E., Schaefer, J. K., Åkerblom, S., and Björn, E.: Terrestrial discharges mediate trophic shifts and enhance methylmercury accumulation in estuarine biota, Sci. Adv., 3, e1601239, https://doi.org/10.1126/sciadv.1601239, 2017.

Jorgenson, M. T. and Grunblatt, J.: Landscape-Level Ecological Mapping of northern Alaska and Field Site Photography, Arctic Landscape Conservation Cooperative, U.S. Fish and Wildlife Service, Fairbanks, Alaska, 2013.

Jorgenson, M. T. and Shur, Y.: Evolution of lakes and basins in northern Alaska and discussion of the thaw lake cycle, J. Geophys. Res., 112, 2006JF000531, https://doi.org/10.1029/2006JF000531, 2007.

Jorgenson, M. T., Shur, Y., Osterkamp, T., Ping, C.-L., and Kanevskiy, M.: Part 1: Environment of the Beaufort Coastal Plain, in: Coastal Region of Northern Alaska - Guidebook to Permafrost and related features, Guidebook 10-1, edited by: Jorgenson, M. T., Division of Geological & Geophysical Surveys, 1–39, 2011.

Kokelj, S. V. and Jorgenson, M. T.: Advances in Thermokarst Research, Permafrost & Periglacial, 24, 108–119, https://doi.org/10.1002/ppp.1779, 2013.

Lenz, J., Jones, B. M., Wetterich, S., Tjallingii, R., Fritz, M., Arp, C. D., Rudaya, N., and Grosse, G.: Impacts of shore expansion and catchment characteristics on lacustrine thermokarst records in permafrost lowlands, Alaska Arctic Coastal Plain, Arktos, 2, 25, https://doi.org/10.1007/s41063-016-0025-0, 2016.

Marzi, R., Torkelson, B. E., and Olson, R. K.: A revised carbon preference index, Organic Geochemistry, 20, 1303–1306, https://doi.org/10.1016/0146-6380(93)90016-5, 1993.

Meyers, P. A.: Organic geochemical proxies of paleoceanographic, paleolimnologic, and paleoclimatic processes, Organic Geochemistry, 27, 213–250, https://doi.org/10.1016/S0146-6380(97)00049-1, 1997.

Miner, K. R., Turetsky, M. R., Malina, E., Bartsch, A., Tamminen, J., McGuire, A. D., Fix, A., Sweeney, C., Elder, C. D., and Miller, C. E.: Permafrost carbon emissions in a changing Arctic, Nat Rev Earth Environ, 3, 55–67, https://doi.org/10.1038/s43017-021-00230-3, 2022.

Mishra, U., Hugelius, G., Shelef, E., Yang, Y., Strauss, J., Lupachev, A., Harden, J. W., Jastrow, J. D., Ping, C.-L., Riley, W. J., Schuur, E. A. G., Matamala, R., Siewert, M., Nave, L. E., Koven, C. D., Fuchs, M., Palmtag, J., Kuhry, P., Treat, C. C., Zubrzycki, S., Hoffman, F. M., Elberling, B., Camill, P., Veremeeva, A., and Orr, A.: Spatial heterogeneity and environmental predictors of permafrost region soil organic carbon stocks, Sci. Adv., 7, eaaz5236, https://doi.org/10.1126/sciadv.aaz5236, 2021.

Obrist, D., Agnan, Y., Jiskra, M., Olson, C. L., Colegrove, D. P., Hueber, J., Moore, C. W., Sonke, J. E., and Helmig, D.: Tundra uptake of atmospheric elemental mercury drives Arctic mercury pollution, Nature, 547, 201–204, https://doi.org/10.1038/nature22997, 2017.

Olefeldt, D., Goswami, S., Grosse, G., Hayes, D., Hugelius, G., Kuhry, P., McGuire, A. D., Romanovsky, V. E., Sannel, A. B. K., Schuur, E. A. G., and Turetsky, M. R.: Circumpolar distribution and carbon storage of thermokarst landscapes, Nat Commun, 7, 13043, https://doi.org/10.1038/ncomms13043, 2016.

Poynter, J.: Molecular stratigraphy: The recognition of paleo-climate signals in organic geochemical data, School of Chemistry, University of Bristol, Bristol, 324 pp., 1989.

Poynter, J. and Eglinton, G.: 14. Molecular Composition of three Sediments from Hole 717C: The Bengal Fan, Proceedings of the Ocean Drilling Program, Scientific Results, 116, 155–161, 1990.

Radke, Matthias., Willsch, Helmut., and Welte, D. H.: Preparative hydrocarbon group type determination by automated medium pressure liquid chromatography, Anal. Chem., 52, 406–411, https://doi.org/10.1021/ac50053a009, 1980.

Rantanen, M., Karpechko, A. Yu., Lipponen, A., Nordling, K., Hyvärinen, O., Ruosteenoja, K., Vihma, T., and Laaksonen, A.: The Arctic has warmed nearly four times faster than the globe since 1979, Commun Earth Environ, 3, 10, https://doi.org/10.1038/s43247-022-00498-3, 2022.

Routh, J., Hugelius, G., Kuhry, P., Filley, T., Tillman, P. K., Becher, M., and Crill, P.: Multi-proxy study of soil organic matter dynamics in permafrost peat deposits reveal vulnerability to climate change in the European Russian Arctic, Chemical Geology, 368, 104–117, https://doi.org/10.1016/j.chemgeo.2013.12.022, 2014.

Rutkowski, C., Lenz, J., Lang, A., Wolter, J., Mothes, S., Reemtsma, T., Grosse, G., Ulrich, M., Fuchs, M., Schirrmeister, L., Fedorov, A., Grigoriev, M., Lantuit, H., and Strauss, J.: Mercury in Sediment Core Samples From Deep Siberian Ice-Rich Permafrost, Front. Earth Sci., 9, 718153, https://doi.org/10.3389/feart.2021.718153, 2021.

Rydberg, J., Klaminder, J., Rosén, P., and Bindler, R.: Climate driven release of carbon and mercury from permafrost mires increases mercury loading to sub-arctic lakes, Science of The Total Environment, 408, 4778–4783, https://doi.org/10.1016/j.scitotenv.2010.06.056, 2010.

Schäfer, I. K., Lanny, V., Franke, J., Eglinton, T. I., Zech, M., Vysloužilová, B., and Zech, R.: Leaf waxes in litter and topsoils along a European transect, SOIL, 2, 551–564, https://doi.org/10.5194/soil-2-551-2016, 2016.

Schirrmeister, L., Grosse, G., Wetterich, S., Overduin, P. P., Strauss, J., Schuur, E. A. G., and Hubberten, H.-W.: Fossil organic matter characteristics in permafrost deposits of the northeast Siberian Arctic, J. Geophys. Res.-Biogeo., 116, G00M02, doi:10.1029/2011jg001647, 2011.

Schirrmeister, L., Grigoriev, M. N., Strauss, J., Grosse, G., Overduin, P. P., Kholodov, A., Guenther, F., and Hubberten, H.-W.: Sediment characteristics of a thermokarst lagoon in the northeastern Siberian Arctic (Ivashkina Lagoon, Bykovsky Peninsula), Arktos, 4, 1–16, https://doi.org/10.1007/s41063-018-0049-8, 2018.

Schuster, P. F., Schaefer, K. M., Aiken, G. R., Antweiler, R. C., Dewild, J. F., Gryziec, J. D., Gusmeroli, A., Hugelius, G., Jafarov, E., Krabbenhoft, D. P., Liu, L., Herman-Mercer, N., Mu, C., Roth, D. A., Schaefer, T., Striegl, R. G., Wickland, K. P., and Zhang, T.: Permafrost Stores a Globally Significant Amount of Mercury, Geophysical Research Letters, 45, 1463–1471, https://doi.org/10.1002/2017GL075571, 2018.

Schuur, E. A. G. and Mack, M. C.: Ecological Response to Permafrost Thaw and Consequences for Local and Global Ecosystem Services, Annu. Rev. Ecol. Evol. Syst., 49, 279–301, https://doi.org/10.1146/annurev-ecolsys-121415-032349, 2018.

Schuur, E. A. G., Vogel, J. G., Crummer, K. G., Lee, H., Sickman, J. O., and Osterkamp, T. E.: The effect of permafrost thaw on old carbon release and net carbon exchange from tundra, Nature, 459, 556–559, https://doi.org/10.1038/nature08031, 2009.

Schuur, E. A. G., Abbott, B. W., Commane, R., Ernakovich, J., Euskirchen, E., Hugelius, G., Grosse, G., Jones, M., Koven, C., Leshyk, V., Lawrence, D., Loranty, M. M., Mauritz, M., Olefeldt, D., Natali, S., Rodenhizer, H., Salmon, V., Schädel, C., Strauss, J., Treat, C., and Turetsky, M.: Permafrost and Climate Change: Carbon Cycle Feedbacks From the Warming Arctic, Annu. Rev. Environ. Resour., 47, 343–371, https://doi.org/10.1146/annurev-environ-012220-011847, 2022.

Smith, S. L., O'Neill, H. B., Isaksen, K., Noetzli, J., and Romanovsky, V. E.: The changing thermal state of permafrost, Nat Rev Earth Environ, 3, 10–23, https://doi.org/10.1038/s43017-021-00240-1, 2022.

Smith-Downey, N. V., Sunderland, E. M., and Jacob, D. J.: Anthropogenic impacts on global storage and emissions of mercury from terrestrial soils: Insights from a new global model, J. Geophys. Res., 115, 2009JG001124, https://doi.org/10.1029/2009JG001124, 2010.

Strauss, J., Schirrmeister, L., Grosse, G., Wetterich, S., Ulrich, M., Herzschuh, U., and Hubberten, H.: The deep permafrost carbon pool of the Yedoma region in Siberia and Alaska, Geophysical Research Letters, 40, 6165–6170, https://doi.org/10.1002/2013GL058088, 2013.

Strauss, J., Schirrmeister, L., Mangelsdorf, K., Eichhorn, L., Wetterich, S., and Herzschuh, U.: Organic-matter quality of deep permafrost carbon – a study from Arctic Siberia, Biogeosciences, 12, 2227–2245, https://doi.org/10.5194/bg-12-2227-2015, 2015.

Strauss, J., Fuchs, M., Hugelius, G., Miesner, F., Nitze, I., Opfergelt, S., Schuur, E., Treat, C., Turetsky, M., Yang, Y., and Grosse, G.: Organic matter storage and vulnerability in the permafrost domain, Encyclopedia of Quaternary Science, 3rd Edition https://doi.org/10.1016/B978-0-323-99931-1.00164-1, 2025.

Strauss, J., Marushchak, M. E., Van Delden, L., Sanders, T., Biasi, C., Voigt, C., Jongejans, L. L., and Treat, C.: Potential nitrogen mobilisation from the Yedoma permafrost domain, Environ. Res. Lett., 19, 043002, https://doi.org/10.1088/1748-9326/ad3167, 2024.

Strauss, J., Biasi, C., Sanders, T., Abbott, B. W., von Deimling, T. S., Voigt, C., Winkel, M., Marushchak, M. E., Kou, D., Fuchs, M., Horn, M. A., Jongejans, L. L., Liebner, S., Nitzbon, J., Schirrmeister, L., Walter Anthony, K., Yang, Y., Zubrzycki, S., Laboor, S., Treat, C., and Grosse, G.: A globally relevant stock of soil nitrogen in the Yedoma permafrost domain, Nature Communications, 13, 6074, doi:10.1038/s41467-022-33794-9, 2022.

Thomas, C. L., Jansen, B., Czerwiński, S., Gałka, M., Knorr, K.-H., Van Loon, E. E., Egli, M., and Wiesenberg, G. L. B.: Comparison of paleobotanical and biomarker records of mountain peatland and forest ecosystem dynamics over the last 2600 years in central Germany, Biogeosciences, 20, 4893–4914, https://doi.org/10.5194/bg-20-4893-2023, 2023.

Voigt, C., Marushchak, M. E., Abbott, B. W., Biasi, C., Elberling, B., Siciliano, S. D., Sonnentag, O., Stewart, K. J., Yang, Y., and Martikainen, P. J.: Nitrous oxide emissions from permafrost-affected soils, Nat Rev Earth Environ, 1, 420–434, https://doi.org/10.1038/s43017-020-0063-9, 2020.

Weintraub, M. N. and Schimel, J. P.: Nitrogen Cycling and the Spread of Shrubs Control Changes in the Carbon Balance of Arctic Tundra Ecosystems, BioScience, 55, 408, https://doi.org/10.1641/0006-3568(2005)055[0408:NCATSO]2.0.CO;2, 2005.

Wendler, G., Moore, B., and Galloway, K.: Strong Temperature Increase and Shrinking Sea Ice in Arctic Alaska, TOASCJ, 8, 7–15, https://doi.org/10.2174/1874282301408010007, 2014.

Wolter, J., Lantuit, H., Wetterich, S., Rethemeyer, J., and Fritz, M.: Climatic, geomorphologic and hydrologic perturbations as drivers for mid- to late Holocene development of ice-wedge polygons in the western Canadian Arctic, Permafrost and Periglacial Processes, 29, 164-181, doi:https://doi.org/10.1002/ppp.1977, 2018.

Wolter, J., Jones, B. M., Fuchs, M., Breen, A., Bussmann, I., Koch, B., Lenz, J., Myers-Smith, I. H., Sachs, T., Strauss, J., Nitze, I., and Grosse, G.: Post-drainage vegetation, microtopography and organic matter in Arctic drained lake basins, Environ. Res. Lett., 19, 045001, https://doi.org/10.1088/1748-9326/ad2eeb, 2024.

Zech, M., Buggle, B., Leiber, K., Marković, S., Glaser, B., Hambach, U., Huwe, B., Stevens, T., Sümegi, P., Wiesenberg, G., and Zöller, L.: Reconstructing Quaternary vegetation history in the Carpathian Basin, SE-Europe, using n-alkane biomarkers as molecular fossils: Problems and possible solutions, potential and limitations, E&G Quaternary Sci. J., 58, 148–155, https://doi.org/10.3285/eg.58.2.03, 2010.

Zheng, Y., Zhou, W., Meyers, P. A., and Xie, S.: Lipid biomarkers in the Zoigê-Hongyuan peat deposit: Indicators of Holocene climate changes in West China, Organic Geochemistry, 38, 1927–1940, https://doi.org/10.1016/j.orggeochem.2007.06.012, 2007.